molecules

MDPI

Article

Synthesis and Characterization of New Ruthenium (II) Complexes of Stoichiometry [Ru(*p*-Cymene)Cl_2L] and Their Cytotoxicity against HeLa-Type Cancer Cells

Marta G. Fuster [1], Imane Moulefera [1], Mercedes G. Montalbán [1], José Pérez [2], Gloria Víllora [1] and Gabriel García [3,*]

[1] Departamento de Ingeniería Química, Facultad de Química, Campus Regional de Excelencia "Campus Mare Nostrum", Universidad de Murcia, 30071 Murcia, Spain
[2] Departamento de Ingeniería Química y Medioambiental, ETSII, Universidad Politécnica de Cartagena, 30203 Cartagena, Spain
[3] Departamento de Química Inorgánica, Facultad de Química, Campus Regional de Excelencia "Campus Mare Nostrum", Universidad de Murcia, 30071 Murcia, Spain
* Correspondence: ggarcia@um.es

Abstract: When the [Ru(*p*-cymene)(μ-Cl)Cl]$_2$ complex is made to react, in dichloromethane, with the following ligands: 2-aminobenzonitrile (2abn), 4-aminobenzonitrile (4abn), 2-aminopyridine (2ampy) and 4-aminopyridine (4ampy), after addition of hexane, the following compounds are obtained: [Ru(*p*-cymene)Cl_2(2abn)] **(I)**, [Ru(*p*-cymene)Cl_2(4abn)] **(II)**, [Ru(*p*-cymene)Cl_2(2ampy] **(III)** and [Ru(*p*-cymene)Cl_2(μ-(4ampy)] **(IV)**. All the compounds are characterized by elemental analysis of carbon, hydrogen and nitrogen, proton nuclear magnetic resonance, COSY ^{1}H-^{1}H, high-resolution mass spectrometry (ESI), thermogravimetry and single-crystal X-ray diffraction (the crystal structure of **III** is reported and compared with the closely related literature of **II**). The cytotoxicity effects of complexes were described for cervical cancer HeLa cells via 3-(4.5-dimethylthiazol-2-yl)-2.5-diphenyltetrazolium bromide (MTT) assay. The results demonstrate a low in vitro anticancer potential of the complexes.

Keywords: ruthenium; complexes; cytotoxicity; anticancer activity; HeLa; MTT assay

Citation: Fuster, M.G.; Moulefera, I.; Montalbán, M.G.; Pérez, J.; Víllora, G.; García, G. Synthesis and Characterization of New Ruthenium (II) Complexes of Stoichiometry [Ru(*p*-Cymene)Cl_2L] and Their Cytotoxicity against HeLa-Type Cancer Cells. *Molecules* **2022**, *27*, 7264. https://doi.org/10.3390/molecules27217264

Academic Editor: Yungen Liu

Received: 8 September 2022
Accepted: 14 October 2022
Published: 26 October 2022

1. Introduction

In addition to *cis*-platinum [1] and other similar compounds such as carbo-platin [2–4] or allyl-platinum [5–7], it has also been shown that numerous ruthenium (II) compounds are able to exhibit similar properties for cancer therapy [8]. Figure 1 presents some of those that lately have received special attention [9–13].

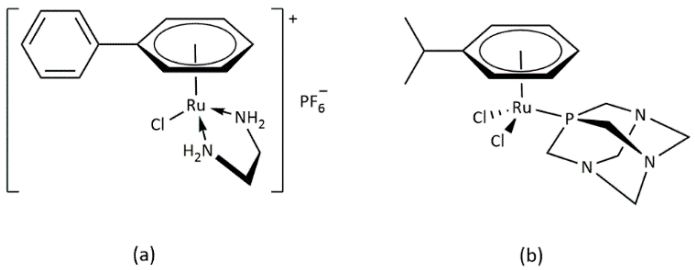

Figure 1. Structures of some antitumor active ruthenium complexes. (**a**) [(η^6-biphenil)Ru(en)Cl]PF_6 and (**b**) [(η^6-p-cymene)Ru(pta)Cl_2].

Recently, the use of platinum-based compounds has been limited because of their lack of cellular selectivity and drug resistance. Ruthenium is attracting the interest of researchers as a promising alternative to platinum-based complexes due to their several

oxidation states, Ru (II), Ru (III) and Ru (IV), and improved cellular selectivity [14]. In this way, ruthenium (II) complexes display excellent structural, photophysical and biological properties, which makes them promising anticancer compounds [15]. The mechanism of action for many ruthenium complexes differs from the DNA-binding mechanism typically associated with platinum compounds, having a wider range of intracellular targets [16]. In addition, ruthenium-based drugs have demonstrated superior therapeutic efficiency in robust metastatic cancers or cisplatin resistant tumors [17].

Some years ago, our research group described the synthesis of the compound [Ru(*p*-cymene)Cl(o-phen)]PF_6, (o-phen = o-phenylenediamine) [18], which has shown to be an excellent antitumor agent [19,20]. Moreover, complexes [Ru(*p*-cymene)Cl_2L], L being one of the following substituted pyridines: 2-fluoro-5-aminopyridine, 5-amino-2-chloropyridine and 2-bromo-5-aminopyridine, have been isolated and characterized and have shown moderate cytotoxicity against lung carcinoma A549 and breast cancer MCF-7 cell lines [21]. Recently, J. Ruiz et al. [22] have described a set of ruthenium (II) complexes containing *p*-cymene, and a C-N ligand with a non-coordinated CHO group, capable of exhibiting anticancer properties towards several human cancer cell lines, including cells of the epithelial ovarian carcinoma A2780, CDDP-resistant ovarian cancer A2780cisR and breast cancer MCF-7. They have also tested the compounds in the non-tumorigenic BGM and CHO cells, finding high selectivity towards cancer cells over normal cells. Ismail et al. [23] have synthesized two new hybrid half-sandwiched Ru(II) arene complexes of a general formula [η^6-(*p*-cymene)Ru(L)Cl] (where L = *1-(Benzazol-2-yl)-3-(thiophen-2-yl) propane-1,3-dione*), which have exhibited significant inhibitory activity against human breast and lung cancer cells (MCF-7 and A549), finding lower IC_{50} values than those of clinical cisplatin drugs. Recently, our group has prepared new compounds of ruthenium (II), neutral and ionic that behave as anticancer agents, especially one of them: [Ru(*p*-cymene)(2amfol)Cl_2];, (2amfol = 2-aminephenol) against HeLa and MCF-7 cells [24].

Nowadays, scientists worldwide have expanded the use of specific features of organometallic ruthenium compounds (e.g., structural diversity, ligand exchangeability, redox and catalytic properties) for medicinal purposes with surprising results. The aim of this work is the synthesis and characterization of organometallic ruthenium compounds, obtained by reacting [Ru(*p*-cymene) Cl(μ-Cl)]$_2$ against potentially bidentate ligands with two donor nitrogen atoms, obtaining the new complexes [Ru(*p*-cymene) Cl_2L]; L = 2abn, 4abn, 2ampy and 4ampy. In addition, a study of their properties as antitumor agents was carried out by MTT assay on HeLa cells.

2. Results and Discussion

Although the ligands used are potentially bidentate, they always act as monodentate across the amine nitrogen (abn) or pyridine nitrogen (ampy). This behavior has been previously observed on ruthenium (II) complexes [18,24]. Only D. S. Pandey et al. have described a related compound in which the CN group acts as a bridge [25].

The four ruthenium (II) complexes shown in Figure 2 were obtained with good yields, and they are air-stable solids that present colors in the yellow–orange range. All of them gave satisfactory analyses of carbon, hydrogen and nitrogen (see Table 1). Moreover, all the isolated complexes are neutral in acetone solutions 5×10^{-4} M [25].

The X-ray diffraction structures of complexes **II** [26] and **III** [27] have been previously described, however, in the case of **II,** no additional data have been presented and, in the case of **III**, in our hands, another polymorph with a different space group is obtained.

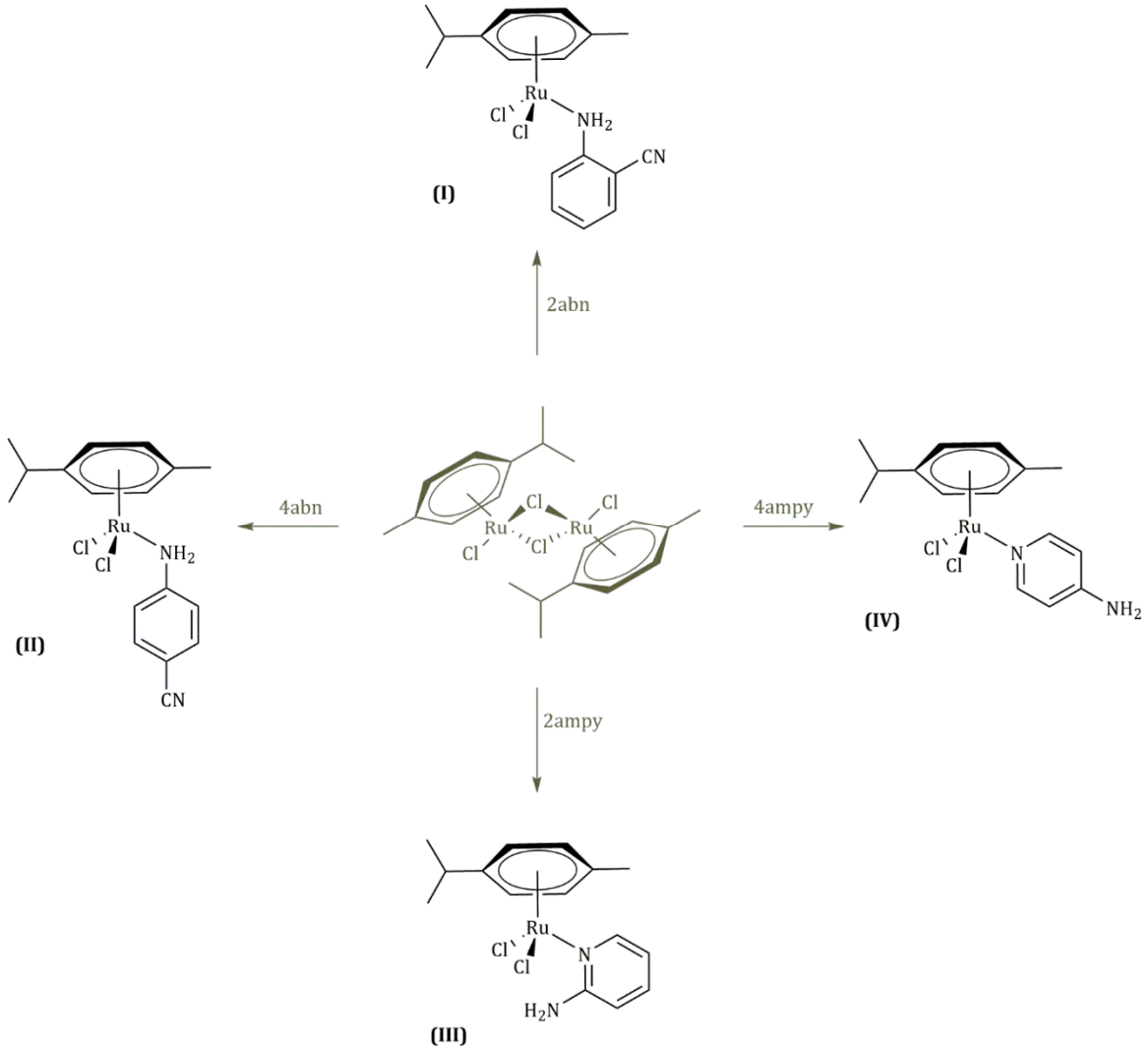

Figure 2. Complexes **I**, **II**, **III** and **IV**.

Table 1. Color, yield, Elemental Analysis, Exact Mass and Decomposition temperatures from complexes **I**, **II**, **III** and **IV**.

Comp.	Color	Yield (%)	Analysis [a] (%)			Exact Mass [a] (g/mol)			M.P. [b] (°C)
			C	H	N	$[M-H]^+$	$[M-Cl]^+$	$[M-2Cl]^+$	
I	Yellow–orange	70	48.09 (48.12)	4.73 (4.75)	6.40 (6.60)		388.8792 (388.8812)	-	69
II	Yellow–orange	90	48.25 (48.12)	4.77 (4.75)	6.53 (6.60)	425.3591 (425.3418)	-	-	90
III	Orange	85	44.86 (45.01)	5.06 (5.04)	6.83 (7.00)	-	-	329.0595 (329.4365)	78
IV	Light Brown	90	44.70 (45.01)	4.87 (5.04)	6.95 (7.00)	-		329.0599 (329.4365)	72

[a] Calculates values in parenthesis. [b] Decomposition temperatures from the thermogravimetric curves.

2.1. Molecular Structure

Complexes exhibit distorted octahedral geometry: three positions occupied by chlorine and N atoms and the three remaining by *p*-cymene ligand. The highest deviation from the ideal 90 degree bond angle is N-RuCl2, 80.17º (**II**) and N-Ru-Cl2, 86.22° (**III**). Most

relevant molecular parameters are shown in Table 2. The difference in the hybridization of coordinated nitrogen explains the difference in Ru-N distances: coordinated N in **II** is sp3 and in **III** is sp (see Figure 3). Both Cl-Ru distances are similar in RuCl2(*p*-cymene) (4-aminobenzonitrile), but in $RhCl_2$(*p*-cymene) (2-aminopyridine), Cl-Rh distances are different (Table 2); the reason is an intramolecular hydrogen bond N-H···Cl that lengthens Rh-Cl(1) distance.

Table 2. Relevant molecular parameters for **II** and **III**.

$RuCl_2$(*p*-Cymene)(4-Aminobenzonitrile)		**$RhCl_2$(*p*-Cymene)(2-Aminopyridine)**	
Ru-N	2.1756(18) Å	Ru-N	2.1693(14) Å
Ru-Cl(1)	2.4260(5) Å	Ru-Cl(1)	2.4545(8) Å
Ru-Cl(2)	2.4219(5) Å	Ru-Cl(2)	2.4153(8) Å
N-Ru-Cl(1)	82.57(5)º	N-Ru-Cl(1)	88.14(3)º
N-Ru-Cl(2)	80.17(5)º	N-Ru-Cl(2)	88.86(3)º
Cl(1)-Ru-Cl(2)	89.261(17)º	Cl(1)-Ru-Cl(2)	86.22(3)º
Ru-Centroide(*p*-cymene)	1.421 Å	Ru-Centroide(*p*-cymene)	1.432 Å
		Hydrogen bond N(2)-H(01)···Cl(1) [Å and º] d(N-H): 0.851(16); d(H···Cl): 2.418(17); d(N···Cl): 3.1917(16); <(NHCl): 151(2).	
Molecular surface	537.2 $Å^2$	Molecular surface	491.6 $Å^2$
Molecular volume	299.9 $Å^3$	Molecular volume	280.8 $Å^3$
Ovality	1.730	Ovality	1.669

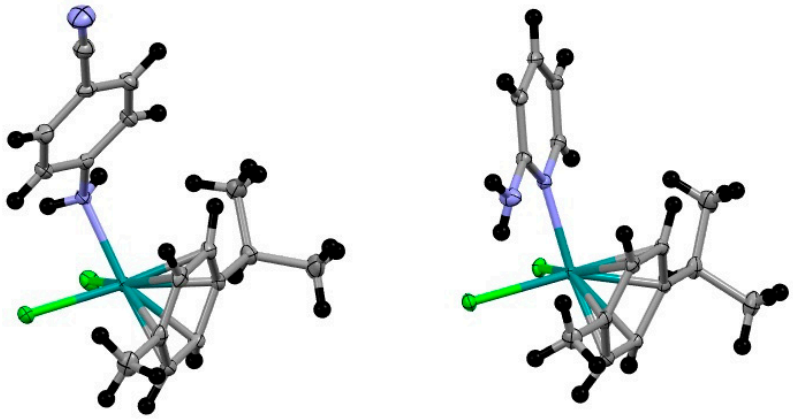

Figure 3. Molecular structure of **II** (**left**) and **III** (**right**).

Difference in molecule surface and volume (Table 2) matches differences in these parameters for ligands 4-aminobenzonitrile and 2-aminopyridine. These ligands also originally differ in ovality.

2.2. Supramolecular Structure

The most relevant features of crystal packing in **II** are shown in Figure 4. The structure consists of infinite chains of molecules linked by N-H···N≡C contacts. In addition, there are C-H···Cl and N-H···Cl contacts. This is confirmed by the Hirshfeld surface (HS) analysis [28–31]. Figure 5 shows the d_{norm} Hirshfeld surface; its associated 2D fingerprint can be decomposed into contributions from N···H/H···N interactions (these make up 13.8% of the surface area of the HS) and H···Cl/Cl···H interactions (21.1%). The Supplementary Materials contains fingerprint plots.

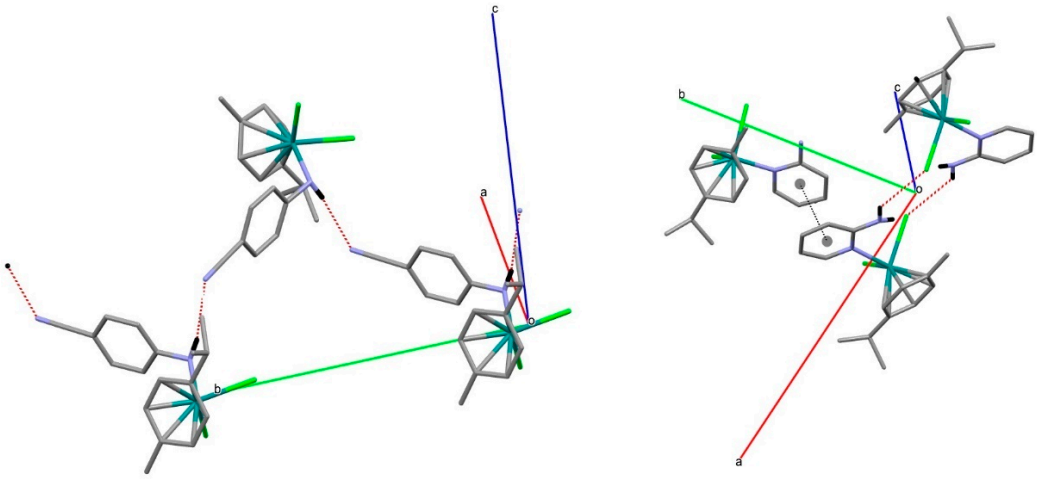

Figure 4. Supramolecular packing in **II** (**left**) and **III** (**right**).

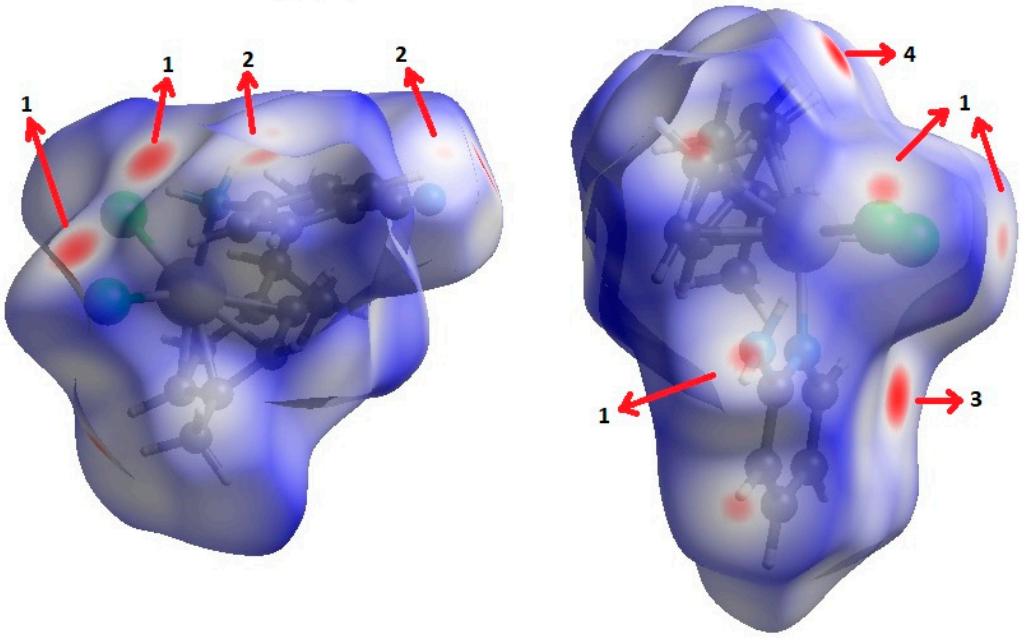

Figure 5. View of the Hirshfeld surfaces mapped over d_{norm} property of **II** (**left**) and **III** (**right**). The labels 1, 2, 3 and 4 represent Cl···H/H···Cl, N···H/H···N, π···π and C-H···π interactions, respectively.

In spite of complex **III** possessing smaller molecular weight, it shows larger density than **II**. This more compact crystal packing for **III** can be explained in part by the π···π stacking interaction between 2ampy ligands (Figure 4) with centroids at 3.695 Å distance. In addition, there are C-H···π and N-H···Cl contacts. Figure 5 shows the d_{norm} Hirshfeld surface; its associated 2D fingerprint can be decomposed into contributions from C···H/H···C interactions (these make up 10.5% of the surface area of the HS), H···Cl/Cl···H interactions (21.8%) and C···C interactions (3.9%). The Supplementary Materials contains fingerprint plots.

Complexes **I** and **II** show absorptions due to ν(CN) in the 2230 cm^{-1} environment that agree that the ligand does not behave as a bridge through nitrile nitrogen. However, the three bands assignable to NH_2 appear between 3200 and 3100 cm^{-1}. The coordination through the pyridine nitrogen atom in **III** and **IV** is evidenced by the displacement of two bands at 604 cm^{-1} (in-plane ring deformation) and 405 cm^{-1} (out-of-plane ring deformation) to higher frequencies (631 and 424 cm^{-1}, respectively). Complexes **I**, **II**, **III**

and **IV** exhibit bands assignable to ν(NH) in the 3400–3100 range, about 100 cm^{-1} below the free ligand [32]. In **I** and **II**, the decrease in NH_2 frequencies is due to the coordination of amine group to the ruthenium atom. However, in the case of **III** and **IV**, where the neutral ligand is bound to the ruthenium via the pyridinic nitrogen, the decrease in NH_2 frequencies may be due to intra-(**III**) or inter-(**IV**) molecular NH_2-Cl interactions. All the isolated compounds show two absorptions assigned to ν(RuCl) at about 290–270 cm^{-1}.

Table 1 also includes the data obtained from their high-resolution mass spectra (ESI), and Table 3 show relevant data from Proton Nuclear Magnetic Resonance. The assignments of the aromatic ring signals of the ligands (2abn and 2ampy) in **I** and **III** were made through COSY ^{1}H-^{1}H experiments.

Table 3. ^{1}H-NMR data of **I**, **II**, **III** and **IV**.

Complex	^{1}H δ(SiMe$_4$) (in CD_2CCl_2)	Ligand Structure
I	7.37–7.28 (m, **Hb** + **Hd**) 6.82 (d, **Ha**, Jab = 8.1Hz) 6.67 (t, **Hc**, Jbc = 8.1Hz) 5.88–5.72 (dd, –C_6**H$_4$**, J = 6.2 Hz) 5.47 (s, *br*, –N**H$_2$**) 2.78 (spt, 1H, –C**H**$(CH_3)_2$, J = 6.9 Hz) 1.61 (s, –C**H$_3$**) 1.30 (d, –CH(C**H$_3$**)$_2$, J = 6.9 Hz)	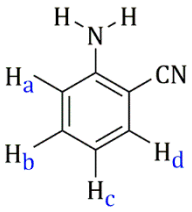
II	7.23 (m, **Ha**) 6.54 (m, **Hb**) 5.75–5.53 (dd, –C_6**H$_4$**, J = 6.2 Hz) 4,72 (s, *br*, –N**H$_2$**) 2.65 (spt, –C**H**$(CH_3)_2$) 2.07 (s, –C**H$_3$**) 1.18 (d, 6H, –CH(C**H$_3$**)$_2$, J = 6.8 Hz)	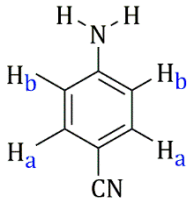
III	8.54 (d, **Hd**, J = 4.8 Hz) 7.42 (pst, **Hc**) 6.62 (pst, **Hb**) 6.58 (d, **Ha**, J = 8.0 Hz) 6.12 (s, *br*, –N**H$_2$**) 5.53–5.31 (dd, –C_6**H$_4$**, J = 6.0 Hz) 2.93 (spt, –C**H**$(CH_3)_2$, J = 7.2 Hz) 1.96 (s, –C**H$_3$**) 1.28 (d, 6H, –CH(C**H$_3$**)$_2$, J = 6.8 Hz)	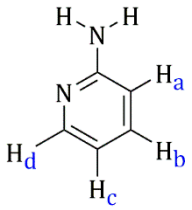
IV	8.33 (d, **Ha**, J = 6.9 Hz) 6.43 (d, **Hb**, J = 6.9 Hz) 4.55 (s, *br*, –N**H$_2$**) 5.37–5.137 (dd, –C_6**H$_4$**, J = 6.0 Hz) 2.90 (spt, –C**H**$(CH_3)_2$, J = 6.9 Hz) 2.12 (s, –C**H$_3$**) 1.27 (d, –CH(C**H$_3$**)$_2$, J = 6.9 Hz)	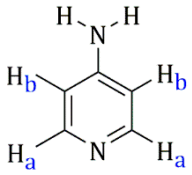

In relation to the mass spectra, under the working conditions used, the molecular peak corresponding to the exact mass is not observed, but others due to $[M\text{-}Cl]^+$ are observed. This type of behavior has been previously observed [22,24].

2.3. In Vitro Cytotoxicity

The in vitro cytotoxic effects of Complex **I**, Complex **II**, Complex **III** and Complex **IV** were assessed with the MTT assay after 48 h of exposure in the HeLa cell line. This cell line was selected due to its origin to determine if any of the complexes have anticancer activity. HeLa cells are derived from a cervical carcinoma and have been widely used in cytotoxicity studies [33]. To study the effects of the complexes, concentrations between 0.031–2 mM were evaluated. As complexes were dissolved in DMSO (0.5% *v*/*v*), this solvent without

complex was used at the same concentration as the control. Cells without treatment were used as the control (data not revealed). After 48 h of incubation with several concentrations of the complexes, the cell viability decreased very slowly or remained almost constant as the concentration increased (Figure 6). However, Complex IV was more cytotoxic than the others, revealing an IC_{50} value, defined as the minimal concentration of a drug that is required for 50% inhibition in vitro of 1.6 ± 0.004 mM.

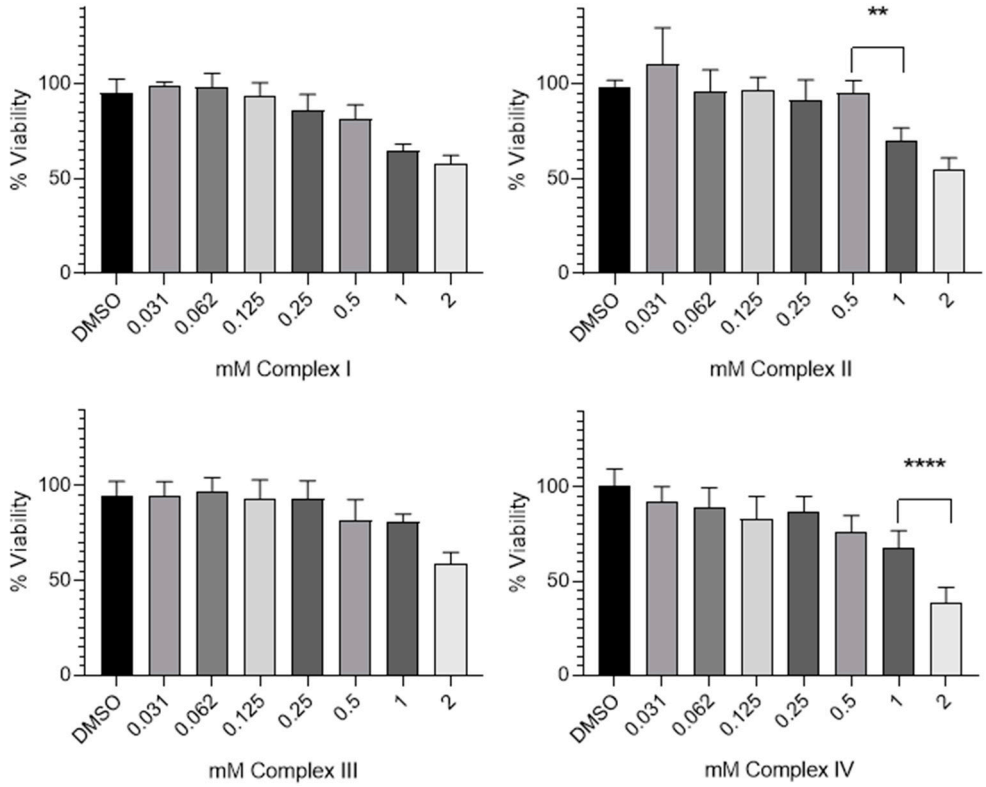

Figure 6. Cytotoxicity effect of Complex **I**, Complex **II**, Complex **III** and Complex **IV** on HeLa cell line. Data are expressed as percentage of cell viability ± SD versus concentration. ** indicates $p < 0.01$ and **** indicates $p < 0.0001$, compared with the adjacent column.

Table 4 shows the cytotoxicity expressed as IC_{50} mean values (mM) of the complexes synthesized and cisplatin exposed to HeLa cells for 48 h. As can be seen, the cytotoxic potency is negligible on the HeLa cell line studied.

Table 4. Cytotoxicity expressed as IC_{50} mean values (mM) of the complexes synthesized and cisplatin exposed to HeLa cells for 48 h.

Compound	IC_{50}, mM
Complex **I**	>2
Complex **II**	>2
Complex **III**	>2
Complex **IV**	1.60 ± 0.004
cisplatin	0.06 ± 0.002

3. Materials and Methods

The solvents were dried by conventional methods. The ligands were commercial-grade chemicals and [Ru(*p*-cymene)Cl_2]$_2$ were prepared by the method published in [34]. ^{1}H NMR spectra were recorder on a Bruker Advance 200, 300 or 400 MHz instrument. IR spectra were recorded on a 100 FT-IR Spectrometer as Nujol mulls. The C, H and N analyses were obtained with a LECO CNHS-932 elemental microanalyzer. Thermal decomposition

studies were carried out on a simultaneous analyzer TGA-DTA of TA Instruments. High-resolution (HR)-ESI-MS spectrometry was realized by HPLC Spectrometer/MS TOF Agilent Model 6220.

3.1. X-ray Data Collection, Structure Solution and Refinement for II and III

Diffraction data were collected on a Bruker D8 QUEST diffractometer with monochromated Mo-Kα radiation (Kα = 0.71073 Å), performing ω and φ scans at 100(2) K. SADABS 2016/2 absorption correction was performed (Bruker (2016). *APEX3*, *SADABS* and *SAINT*. Bruker AXS Inc., Madison, Wisconsin, USA)

The structures were solved by direct methods [35] and refined anisotropically on F2 using the program SHELXL-2018 [36]. CIF files were validated using checkCIF [37]. Numerical details are presented in Table 5. Hydrogen atoms bound to C were located at geometrically idealized positions and were allowed to ride on the parent atoms; hydrogen atoms bound to N atoms were discernible from difference-Fourier maps and were subsequently refined with N-H distance restraints. Crystal data for **II** were reported previously [26]; we collected data at low temperature in order to achieve a more precise structural study.

Table 5. X-ray Data Collection Parameters for **II** and **III**.

	II	**III**
formula	$C_{17}H_{20}Cl_2N_2Ru$	$C_{15}H_{20}Cl_2N_2Ru$
fw	424.32	400.30
cryst color, habit	orange, prism	orange, prism
cryst size (mm)	0.090 × 0.050 × 0.030	0.18 × 0.07 × 0.04
cryst syst	monoclinic	monoclinic
space group	P21/n (#14)	P21/c (#14)
a (Å)	8.9362(9)	16.509(7)
b (Å)	12.8438(12)	13.112(5)
c (Å)	14.9730(16)	7.167(2)
α (°)	90	90
β (°)	91.063(4)	93.90(2)
γ (°)	90	90
V (Å^3)	1718.2(3)	1547.8(10)
Z value	4	4
D_{calcd} (g/cm^3)	1.640	1.718
F_{000}	856	808
no. of reflns measd	37,748	69,142
no. of observations	5265	4719
no. of variables	208	192
R1	0.0271	0.0180
wR2	0.0563	0.0434
goodness of fit	1.050	0.903

The generated Hirshfeld surfaces and the associated 2D fingerprint plots are extracted using the CrystalExplorer17 software [38].

3.2. Synthesis of the Complexes

These were prepared according to the following procedure, very similarly to reference [18]. To a dichloromethane (15 mL) solution of [(*p*-cymene)$RuCl_2$]$_2$ (0.4902 mmol), the appropriate ligand (0.9804 mmol for **I**, **II** and **III**; and 0.4902 mmol for **IV**) was added. The resulting suspension was stirred for 1 h and then was concentrated. The solid obtained was separated by filtration, crystallized from dichloromethane/ether and repeatedly washed with diethyl ether.

The crystals used for X-ray diffraction were obtained by slow diffusion of hexane over solutions of **II** and **III** in dichloromethane.

3.3. Cytotoxicity Assays

3.3.1. Cell Culture

Human cervical cancer cells (HeLa) were acquired from the American Type Tissue Culture Collection (ATCC, USA). Cell lines were maintained in the Dulbecco's Modified Eagle Medium (DMEM) with a low content of glucose (1 g/L) supplemented with 10% (*v*/*v*) fetal bovine serum (FBS), 1 mM glutamax, 1% antibiotics (penicillin-streptomycin) and 1 mM pyruvate. Cells were subcultured, and medium was changed once a week. A total of 0.25% trypsine-0.25 mM EDTA was used.

3.3.2. MTT Assay

A total of 3000 cells/well of HeLa carcinoma cell line were seeded onto 96-well plates and incubated at 37 °C in 5% CO_2. After 24 h, the culture medium of each well was replaced with fresh medium, and cells were treated with different concentrations of Complex **I**, Complex **II**, Complex **III** and Complex **IV**; these solutions were diluted in DMSO to obtain a maximum concentration per well of 2 mM. In each experiment, growth medium without nanoparticles was used as a control. Cells were incubated at 37 °C for 48 h. Then, the media were removed and 200 µL of 1% MTT (3-(4,5-dimethylthiazol-2-yl)-2,5-diphenyltetrazolium bromide) was added. After 4 h of incubation, the MTT was removed and 100 µL of dimethyl sulfoxide DMSO was added. The absorbance was measured at 560 nm in a microplate reader Fluostar Omega spectrophotometer. Each sample was tested in three independent sets with triplicate points.

4. Conclusions

Four ruthenium(II) complexes were designed and synthesized, namely [Ru(*p*-cymene)Cl_2(2abn)] **(I)**, [Ru(*p*-cymene)Cl_2(4abn)] **(II)**, [Ru(*p*-cymene)Cl_2(2ampy] **(III)** and [Ru(*p*-cymene)Cl_2(µ-(4ampy)] **(IV)**. Good yields were obtained, and all are air-stable solids exhibited colors in the yellow–orange range. All the compounds were fully characterized by elemental analysis of carbon, hydrogen and nitrogen, proton nuclear magnetic resonance, COSY ^{1}H-^{1}H, high-resolution mass spectrometry (ESI), thermogravimetry and single-crystal X-ray diffraction. Furthermore, the cytotoxic effect of the complexes was evaluated against HeLa cells, and cell viability was found to decrease very slowly in all cases. Only complex IV was more cytotoxic than the others, but it presented a much higher IC_{50} than cisplatin. However, although the results of the synthesized complexes do not show high cytotoxicity values against HeLa cells compared with cisplatin, further studies on the synthesis and characterization of ruthenium complexes are certainly very useful to be able to relate the structures to their unique and versatile biochemical properties.

Supplementary Materials: The following supporting information can be downloaded at: https://www.mdpi.com/article/10.3390/molecules27217264/s1, NMR spectra; Hirshfeld Surface analysis for Complexe II and for Complexe III.

Author Contributions: Methodology, G.V., J.P., M.G.F. and M.G.M.; investigation, M.G.F., I.M. and M.G.M.; Supervision, J.P., G.V. and G.G. All authors have read and agreed to the published version of the manuscript.

Funding: This work has been partially supported by the grant ref. PID2020-113081RB-I00 funded by MCIN/AEI/10.13039/501100011033 and part of the grant ref. 20977/PI/18 funded by the research support program of the Seneca Foundation of Science and Technology of Murcia, Spain. Marta G. Fuster acknowledges support from FPI grant (Ref. PRE2018-086441) funded by MCIN/AEI/10.13039/501100011033 and by "ESF Investing in your future" Imane Moulefera acknowledges support from the Spanish Ministry of Universities under "Margarita Salas program", financed by Next Generation EU.

Institutional Review Board Statement: Not applicable.

Informed Consent Statement: Not applicable.

Data Availability Statement: Data are contained in the article and in Supplementary Materials.

Conflicts of Interest: The authors declare no conflict of interest.

Sample Availability: Samples of the compounds are available from the authors.

References

1. Rosenberg, B.; Vancamp, L.; Trosko, J.E.; Mansour, V.H. Platinum Compounds: A New Class of Potent Antitumour Agents. *Nature* **1969**, *222*, 385–386. [CrossRef] [PubMed]
2. Cleare, M.J.; Hoeschele, J.D. Anti-Tumour Platinum Compounds. Relationship Between Structure and Activity. *Platin. Met. Rev.* **1973**, *17*, 2–13.
3. Cleare, M.J.; Hoeschele, J.D. Studies on the antitumor activity of group VIII transition metal complexes. Part I. Platinum (II) complexes. *Bioinorg. Chem.* **1973**, *2*, 187–210. [CrossRef]
4. Boulikas, T.; Vougiouka, M. Cisplatin and platinum drugs at the molecular level (Review). *Oncol. Rep.* **2003**, *10*, 1663–1682. [CrossRef]
5. Kelland, L. The resurgence of platinum-based cancer chemotherapy. *Nat. Rev. Cancer* **2007**, *7*, 573–584. [CrossRef]
6. Graham, J.; Mushin, M.; Kirkpatrick, P. Oxaliplatin. *Nat. Rev. Drug Discov.* **2004**, *3*, 11–12. [CrossRef]
7. Wang, D.; Lippard, S.J. Cellular processing of platinum anticancer drug. *Nat. Rev. Drug Discov.* **2005**, *4*, 307–320. [CrossRef]
8. Dabrowiak, J.C. *Metals in Medicine*, 2nd ed.; John Wiley & Sons: Hoboken, NJ, USA, 2017.
9. Morris, R.E.; Aird, R.E.; del Socorro Murdoch, P.; Chen, H.; Cummings, J.; Hughes, N.D.; Parsons, S.; Parkin, A.; Boyd, G.; Jodrell, D.I.; et al. Inhibition of cancer cell growth by ruthenium (II) arene complexes. *J. Med. Chem.* **2001**, *44*, 3616–3621. [CrossRef]
10. Bugarcic, T.; Habtemariam, A.; Stepankova, J.; Heringova, P.; Kasparkova, J.; Deeth, R.J.; Johnstone, R.D.L.; Prescimone, A.; Parkin, A.; Parsons, S.; et al. The Contrasting Chemistry and Cancer Cell Cytotoxicity of Bipyridine and Bipyridinediol Ruthenium(II) Arene Complexes. *Inorg. Chem.* **2008**, *47*, 11470–11486. [CrossRef]
11. Bugarcic, T.; Nováková, O.; Halámiková, A.; Zerzánková, L.; Vrána, O.; Kašpárková, J.; Habtemariam, A.; Parsons, S.; Sadler, P.J.; Brabec, V. Cytotoxicity, cellular uptake, and DNA interactions of new monodentate ruthenium(II) complexes containing terphenyl arenes. *J. Med. Chem.* **2008**, *51*, 5310–5319. [CrossRef]
12. Scolaro, C.; Chaplin, A.B.; Hartinger, C.G.; Bergamo, A.; Cocchietto, M.; Keppler, B.K.; Sava, G.; Dyson, P.J. Tuning the hydrophobicity of ruthenium(II)-arene (RAPTA) drugs to modify uptake, biomolecular interactions and efficacy. *Dalt. Trans.* **2007**, *2*, 5065–5072. [CrossRef] [PubMed]
13. Wee, H.A.; Dyson, P.J. Classical and non-classical ruthenium-based anticancer drugs: Towards targeted chemotherapy. *Eur. J. Inorg. Chem.* **2006**, *2006*, 4003–4018. [CrossRef]
14. Zeng, J.; Zhao, Y.; Li, K.; Long, D.; Li, W.; Liang, L. A coordinated ruthenium-rifampicin complex reprogramming the colon carcinoma micro-environment mediated by modulation of p53/AkT/mTOR/VEGF pathway. *Toxicol. Appl. Pharmacol.* **2021**, *426*, 115618. [CrossRef]
15. Shen, J.; Rees, T.W.; Ji, L.; Chao, H. Recent advances in ruthenium(II) and iridium(III) complexes containing nanosystems for cancer treatment and bioimaging. *Coord. Chem. Rev.* **2021**, *443*, 214016. [CrossRef]
16. Coverdale, J.P.C.; Laroiya-McCarron, T.; Romero-Canelón, I. Designing ruthenium anticancer drugs: What have we learnt from the key drug candidates? *Inorganics* **2019**, *7*, 31. [CrossRef]
17. Lakshmi, B.A.; Reddy, A.S.; Sangubotla, R.; Hong, J.W.; Kim, S. Ruthenium(II)-curcumin liposome nanoparticles: Synthesis, characterization and their effects against cervical cancer. *Colloids Surf. B Biointerfaces* **2021**, *204*, 111773. [CrossRef]
18. García, G.; Solano, I.; Sánchez, G.; Santana, M.D.; López, G.; Casabó, J.; Molins, E.; Miravitlles, C. Reactivity of [(η^6-arene)RuCl(μ-Cl)$_2$] towards some potentially bidentate ligands. Molecular structure of [(η^6-*p*-cymene)RuCl(taz)]PF_6 (*p*-cymene = *p*-MeC_6H_4CH-Me_2; taz = 2,6-dimethy. *J. Organomet. Chem.* **1994**, *467*, 119–126. [CrossRef]
19. Habtemariam, A.; Sadler, P.J. Ruthenium Compounds. U.S. Patent Application No. US7241913B2, 10 July 2007.
20. Iida, J.; Bell-Loncella, E.T.; Purazo, M.L.; Lu, Y.; Dorchak, J.; Clancy, R.; Slavik, J.; Cutler, M.L.; Shriver, C.D. Inhibition of cancer cell growth by ruthenium complexes. *J. Transl. Med.* **2016**, *14*, 48. [CrossRef]
21. Yan, X.-W.; Xie, Y.-R.; Jin, Z.-M.; Hu, M.-L.; Zhou, L.-P. Three Arene-Ru(II) compounds of 2-halogen-5-aminopyridine: Synthesis, characterization and cytotoxicity. *Appl. Organomet. Chem.* **2017**, *32*, e3923. [CrossRef]
22. Ballester, F.J.; Ortega, E.; Porto, V.; Kostrhunova, H.; Davila-Ferreira, N.; Bautista, D.; Brabec, V.; Domínguez, F.; Santana, M.D.; Ruiz, J. New half-sandwich ruthenium(ii) complexes as proteosynthesis inhibitors in cancer cells. *Chem. Commun.* **2019**, *55*, 1140–1143. [CrossRef]
23. Ismail, L.A.; Alfaifi, M.Y.; Elbehairi, S.E.I.; Elshaarawy, R.F.M.; Gad, E.M.; El-Sayed, W.N. Hybrid organoruthenium(II) complexes with thiophene-β-diketo-benzazole ligands: Synthesis, optical properties, CT-DNA interactions and anticancer activity. *J. Organomet. Chem.* **2021**, *949*, 121960. [CrossRef]
24. Pujante-Galian, M.A.; Pérez, S.A.; Montalbán, M.G.; Carissimi, G.; Fuster, M.G.; Víllora, G.; García, G. *p*-Cymene Complexes of Ruthenium (II) as Antitumor Agents. *Molecules* **2020**, *55*, 5063. [CrossRef] [PubMed]
25. Gupta, D.K.; Sahay, A.N.; Pandey, D.S.; Narendra, K.J.; Sharma, P.; Espinosa, G.; Cabrera, A.; Puerta, M.C.; Valerga, P. Synthesis, characterization, reactivity and structure of some mono and binuclear (η6-*p*-cymene)ruthenium(II) complexes. *J. Organomet. Chem.* **1998**, *568*, 13–20. [CrossRef]

26. Cheng, B.; Tehrani, A.; Hu, M.-L.; Morsali, A. Supramolecular assemblies of Ru(II) organometallic half-sandwich complexes. *CrystEngComm* **2014**, *16*, 9125–9134. [CrossRef]
27. Aronson, R.; Elsegood, M.R.J.; Steed, J.W.; Tocher, D.A. The reactions of $[Ru(\eta^6\text{-arene})Cl_2]_2$ compounds with a series of aminopyridine ligands: X-ray crystal structures of $[Ru(\eta^6\text{-}1,4\text{-}MeC_6H_4CHMe_2)Cl_2(NC_5H_4NH_2)]$ and $[Ru(\eta^6\text{-}C_{16}H_{16})Cl_2(NC_5H_4NH_2)]$. *Polyhedron* **1991**, *10*, 1727–1732. [CrossRef]
28. McKinnon, J.J.; Spackman, M.A.; Mitchell, A.S. Novel tools for visualizing and exploring intermolecular interactions in molecular crystals. *Acta Cryst.* **2004**, *60*, 627–668. [CrossRef]
29. Spackman, M.A.; Jayatilaka, D. Hirshfeld surface analysis. *CrystEngComm* **2009**, *11*, 19–32. [CrossRef]
30. Spackman, M.A.; McKinnon, J.J. Fingerprinting intermolecular interactions in molecular crystals. *CrystEngComm* **2002**, *4*, 378–392. [CrossRef]
31. Khan, B.A.; Hamdani, S.S.; Ahmed, M.N.; Hameed, S.; Ashfaq, M.; Ahmed, M.S.; Ibrahim, M.A.A.; Sidhom, P.A. Synthesis, X-ray diffraction analysis, quantum chemical studies and α-amylase inhibition of probenecid derived S-alkylphthalimide-oxadiazole-benzenesulfonamide hybrids. *J. Enzym. Inhib. Med. Chem.* **2022**, *37*, 1464–1478. [CrossRef]
32. Nakamoto, K. *Infrared and Raman Spectra of Inorganic and Coordination Compounds: Part B: Applications in Coordination, Organometallic and Bioinorganic Chemistry*, 6th ed.; John Wiley & Sons: Hoboken, NJ, USA, 2008; ISBN 9780470405888.
33. Fuster, M.G.; Montalbán, M.G.; Carissimi, G.; Víllora, G. Improving Anticancer Therapy with Naringenin-Loaded Silk Fibroin Nanoparticles. *Nanomaterials* **2020**, *10*, 718. [CrossRef]
34. Bennett, M.A.; Huang, T.N.; Matheson, T.W.; Smith, K. *Inorganic Synthesis*; John Wiley & Sons: Hoboken, NJ, USA, 1982; Volume 21, pp. 74–77.
35. Sheldrick, G.M. Crystal structure refinement with SHELXL. *Acta Crystallogr. Sect. C Struct. Chem.* **2015**, *71*, 3–8. [CrossRef] [PubMed]
36. Sheldrick, G.M. A short history of SHELX. *Acta Crystallogr. Sect. A Found. Crystallogr.* **2007**, *64*, 112–122. [CrossRef] [PubMed]
37. International Union of Crystallography. checkCIF. Available online: https://checkcif.iucr.org/ (accessed on 13 September 2022).
38. Spackman, P.R.; Turner, M.J.; McKinnon, J.J.; Wolff, S.K.; Grimwood, D.J.; Jayatilaka, D.; Spackman, M.A. A program for Hirshfeld surface analysis, visualization and quantitative analysis of molecular crystals. *J. Appl. Crystallogr.* **2021**, *54*, 1006–1011. [CrossRef] [PubMed]